Research Article | Vol. 29, No. 11 / 24 May 2021 / Optics Express 17464
Optics EXPRESS

Digital compensation of imperfect pump counter-phasing induced phase distortion in optical phase conjugation of high-order QAM

TU T. NGUYEN,[1,2,4] SONIA BOSCOLO,[1,5] ABDALLAH A. I. ALI,[1] STYLIANOS SYGLETOS,[1] SHIGEHIRO TAKASAKA,[3] RYUICHI SUGIZAKI,[3] AND ANDREW D. ELLIS[1]

[1]*Aston Institute of Photonic Technologies, Aston University, Aston Triangle, Birmingham B4 7ET, UK*
[2]*Infinera Pennsylvania, 7360 Windsor Dr, Allentown, PA 18106, USA*
[3]*Furukawa Electric Co. Ltd., 6 Yawata-kaigandori, Ichihara, Chiba, 290-8555, Japan*
[4]*t.nguyen14@aston.ac.uk*
[5]*s.a.boscolo@aston.ac.uk*

Abstract: We propose a new two-stage digital signal processing scheme to suppress the phase distortion that arises from imperfect pump counter-phasing in a dual-pump fibre-based optical phase conjugation system. We demonstrate experimentally and numerically a signal-to-noise ratio improvement of more than 4 dB relative to conventional phase noise compensation, when the proposed scheme is used with 16/64/256 quadrature-amplitude modulation signals at pump-phase mismatch values as large as 8°.

1. Introduction

Optical phase conjugation (OPC) is gaining increasing attention as an all-optical technique that can enable the simultaneous compensation of chromatic dispersion and fibre Kerr nonlinearity induced distortions in optical communication systems through mid-span spectral inversion [1,2]. However, a major limitation to the implementation of fibre-based OPC devices relying on four-wave mixing (FWM) is the need to suppress stimulated Brillouin scattering, which limits the forward propagating pump power, restricting the wanted nonlinear effect [3,4]. The most common approach to allow the pump power to be increased is by modulating the pump phase thereby reducing the power spectral density. Typical waveforms demonstrated for pump dithering include combinations of well-chosen sinusoidal tones [5], pseudorandom binary sequences [6] and white noise, where the first phase modulation format is the most commonly used in practice as it enables control of the details of the laser spectrum. However, this approach itself is a source of problems. For a single-pump scheme, it introduces phase distortions on the conjugated signal (idler) that can severely degrade the performance of phase-modulation signal formats [7]. Theoretically, the phase modulation transfer from the pump to the idler can be fully suppressed by using a dual-pump scheme in which the two pumps are modulated using complementary phase patterns [8,9]. However, this approach requires precise adjustment of the phase and amplitude of the modulating signals, which is difficult to achieve in practice. Therefore, small deviations from the ideal case commonly exist, and should be accounted for in the design of the optical transceivers for phase-modulated communication systems deploying OPC.

Several digital signal processing (DSP) techniques have been developed to estimate and compensate the phase noise (PN) induced by laser non-zero spectral width in coherent optical systems [10–13]. However, these methods as standalone cannot efficiently counteract the deterministic effects of imperfections in the pump-phase modulation scheme of OPC systems

#418386 https://doi.org/10.1364/OE.418386
Journal © 2021 Received 23 Dec 2020; revised 17 Mar 2021; accepted 23 Mar 2021; published 21 May 2021

Optics EXPRESS

where the idler phase modulation is strong. This is because of either their decision-directed operation [11] or the requirement of a relatively constant PN evolution over a long time window [13]. In [14], the authors demonstrated a compensation algorithm for the phase distortion originating from the pump phase modulation in a single-pump parametric wavelength converter. The method uses peak searching in the frequency domain (mth-power operation) to estimate the parameters of the sinusoidal phase distortion from the phase of the idler symbols before recovering the carrier phase. However, this technique is not suitable to high-order signal modulation formats because a mth-power based algorithm performs poorly with non-uniform phase distribution signals [15]. Further, the usability of a peak searching algorithm with dual-pump FWM-based devices with counter-phased pumps is questionable because the residual phase modulation is low and the spectrum has many components. Notwithstanding, the method reported in [14] may still be deployed in OPC systems with severe pump phasing-induced phase distortion as a coarse stage of PN compensation.

In this paper, we develop a new method for compensating the phase distortion caused by deviations from ideal counter-phasing of the pumps in the OPC of high-order quadrature-amplitude modulation (QAM) signals, which we implement using a two-stage design. After conventional PN compensation, in the second stage for each dominant spectral component (corresponding to the known phase-modulation frequencies) we perform a least squared error fit to the required tone amplitude and angle. The proposed scheme is verified numerically and experimentally with 16-, 64- and 256-QAM signals. The large improvement in signal-to-noise ratio (SNR) achieved by the second stage compared to the conventional PN compensation stage indicates that it is possible to relax the requirement of pump counter-phasing calibration in the OPC implementation.

2. Phase distortion from OPC and compensation algorithm

2.1. OPC model

In our numerical model of OPC, we consider a dual-pump unidirectional system. The complex field envelope of the pump waves, which is assumed free from amplitude fluctuations, can be expressed as

$$A_{pi}(t) = |A_{pi}|e^{i[\delta\phi_i(t)+\phi_{mi}(t)]}, \quad i = 1, 2 \tag{1}$$

where the phase fluctuation $\delta\phi_i$ exhibits a simple Brownian motion (Wiener process) in which the increments obey a Gaussian probability distribution [16]. This model implies that the power spectrum of the wave has a Lorentzian shape, which is a general assumption for all known continuous-wave lasers with a finite linewidth [17]. Likewise with the OPC device used in [18], the pumps are independently phase-modulated with two sinusoidal signals with frequencies $f_1 = \omega_1/(2\pi) = 60\,\text{MHz}$ and $f_2 = \omega_2/(2\pi) = 600\,\text{MHz}$. We account for nonlinearities of the radio-frequency (RF) power amplifiers by using a third-order polynomial model [19] for the amplifier's response to the two-tone input signal. The output waveforms from the amplifiers are then filtered using low-pass filters with a 3-dB cutoff frequency of 700 MHz likewise with the experiment. Therefore, the pump phase modulations may be written in the form

$$\begin{gathered}\phi_{mi}(t) = \int \mathrm{d}\tau\, h(t-\tau)\left[\alpha_1 f_i(\tau) + \alpha_2 f_i(\tau)^2 + \alpha_3 f_i(\tau)^3\right], \quad i = 1, 2 \\ f_1(t) = (m+\delta m)\left[\cos(\omega_1 t + \delta\theta) + \cos(\omega_2 t + \delta\theta)\right], \quad f_2(t) = m\left[-\cos(\omega_1 t) - \cos(\omega_2 t)\right]\end{gathered} \tag{2}$$

where the α's are the coefficients of the polynomial response of the amplifiers, $h(t)$ is the impulse response of the filters, m is the modulation index, the modulation-index mismatch δm represents possibly different modulation indices, and the pump-phase mismatch $\delta\theta$ accounts for a non-ideal phase shift. Since the envelope of the idler's field is proportional to the product $A_{p1} \cdot A_{p2}$ [20], the general pump phase contribution to the idler phase is given by $\phi_{p\to i} = \phi_{p1} + \phi_{p2}$, where $\phi_{pi} = \delta\phi_i + \phi_{mi}$. It is easy to see that the pump-phase modulation contribution only vanishes for

Optics EXPRESS

ideal counter-phasing, $\delta m = \delta\theta = 0$, under the assumption of linear amplifier's response. One may also see from Eq. (2) that, assuming a linear amplifier's response and $\delta\theta \ll 1$, in all cases but $\delta m = \delta\theta = 0$ the idler is modulated with f_1 and f_2 and an effective modulation index that increases linearly with the modulation-index and pump-phase mismatches. Ideal counter-phasing is difficult to achieve in practice. In our numerical simulations, we use $m = 1.3$ rad, $\delta m = 0.01$ rad, $\alpha_1 = 1$, $\alpha_2 = 0.007$, $\alpha_3 = 0.005$, and we vary the pump phase-mismatch parameter $\delta\theta$ to control the deviation of the pump phases from optimum counter-phasing.

Each pump is combined with amplified spontaneous emission noise from an amplifier with a noise figure of ~ 4.5 dB, and an optical band-pass filter with a 3-dB bandwidth of 2 nm is used to suppress the out-of-band noise around it. The pump waves, orthogonally polarised, are combined with the signal, polarised at a 45° angle with respect to either pump, and then sent to a highly nonlinear fibre (HNLF). The numerical simulations of the field propagation in the fibre are based on two incoherently coupled nonlinear Schrödinger equations (Manakov system) [21]. The simulation parameters are adjusted slightly from the nominal values (Section 3) in order to match the experimentally observed conversion efficiency.

2.2. Two-stage PN compensation scheme

Figure 1 shows the conceptual model of the various sources of PN in the OPC transceiver being studied. At the transmitter, the complex-valued QAM symbols $x[k]$ are passed through a pulse-shaping filter with impulse response $p(t)$, and modulated optically. The optical signal is then transmitted through a dual-pump OPC module, and the conjugated output signal from the OPC device is mixed with a local oscillator at the coherent receiver. The received signal $y(t)$ is pulse-shaped by the same filter used at the transmitter, sampled at the sample time T_s (symbol period) and injected into the PN compensation module. For simplicity, perfect timing recovery, ideal synchronisation and zero frequency-offset are assumed. The contributions of the transmitter, OPC pumps and receiver to the PN of the received signal are represented by $\delta\phi_{\text{tx}}(t)$, $[\delta\phi_i(t) + \phi_{mi}(t)]$, $i = 1, 2$, and $\delta\phi_{\text{rx}}(t)$, respectively, in the diagram. The phase-distorted received signal at the input to the PN compensation unit, then, can be written in the form

$$y[k] = x[k]\mathrm{e}^{i(\overbrace{\delta\phi[k]}^{(1)} + \overbrace{\phi_m[k]}^{(2)})} + \varepsilon[k], \tag{3}$$

where $\varepsilon[k]$ is the additive white circularly symmetric Gaussian noise (e.g., amplified spontaneous emission noise) present in the system. The first phase term represents the Wiener random laser PN: $\delta\phi[k] = \delta\phi[k-1] + W[k]$, where $W[k] \sim \mathcal{N}(0, 2\pi\delta\nu T_s)$ and $\delta\nu$ is the combined spectral linewidth of the system (total linewidth of transmit, receive and pump lasers) [10]. The second phase term $\phi_m[k] = \phi_{m1}[k] + \phi_{m2}[k]$ represents the deterministic phase distortion generated by imperfect pump counter-phasing (Eq. (2)). The aim of our compensation algorithm is to estimate and remove this phase component. To this end, we apply a two-stage procedure, as depicted in Fig. 2(a).

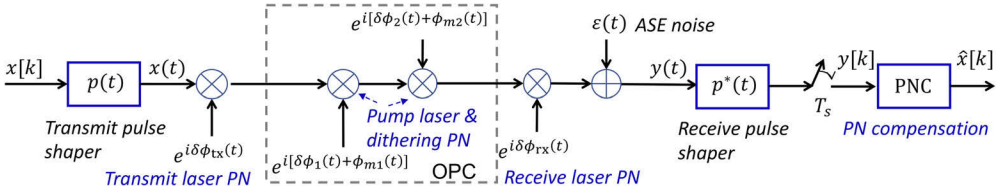

Fig. 1. Conceptual diagram of the OPC transceiver.

Optics EXPRESS

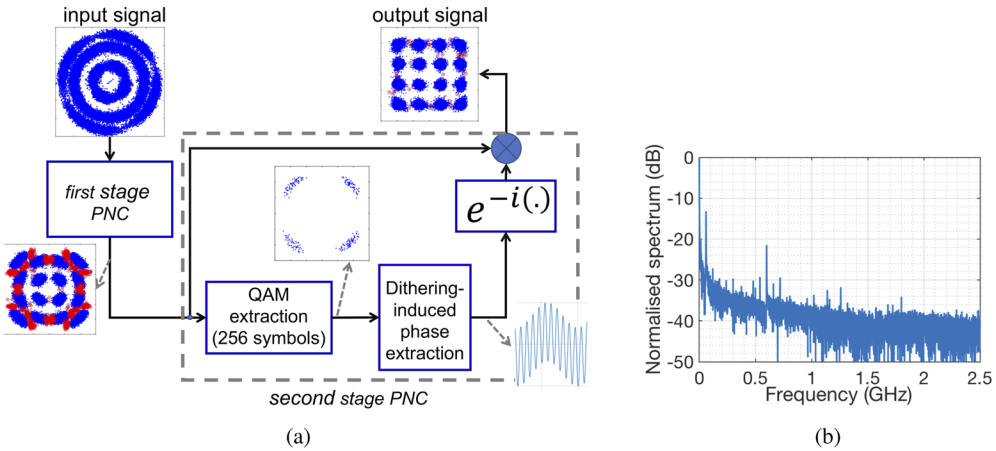

(a) (b)

Fig. 2. (a) Block diagram of the two-stage PN compensation algorithm implementation. The signal constellation diagrams at the input and output of the first stage and the output of the second stage are shown for 16-QAM at a pump-phase mismatch of $\delta\theta = 8^\circ$ and an optical SNR of ~ 36 dB. The red points represent the symbols in error. (b) Corresponding frequency representation of the estimated PN after the first stage for 16-QAM.

The first stage is a feedforward phase estimation block based on the well-known blind phase search (BPS) algorithm [11], the principle of which is as follows. The received signal is rotated by B test carrier phase angles, then all rotated symbols are fed into a decision circuit and the squared distance to the closest constellation point is calculated in the complex plane. In order to remove noise distortions, the distances of $2N + 1$ consecutive test symbols rotated by the same carrier phase are summed up, where N denotes the half width of the linear filter. After filtering, the optimum phase angle is determined by searching the minimum sum of distance values, and the decoded output symbol is selected from the decision-directed symbols by a switch controlled by the index of the minimum distance sum. The accuracy of this carrier recovery algorithm obviously depends on the number of test phase values used. In the algorithm's implementation, we use $B = 32$, 64 and 64 test phase angles for 16-, 64- and 256-QAM, respectively, and the same filter's width of $2N = 12$. When this PN compensation unit is followed by the second block in our scheme, only the stage of phase estimation is used. To visually illustrate the process flow of the proposed scheme, we plot in Fig. 2(a) the constellation diagrams of the 16-QAM signal at the input and output of the first PN compensation stage and the output of the second stage for a pump-phase mismatch of $\delta\theta = 8^\circ$ and an optical SNR of ~ 36 dB. After the BPS-based first stage, the phase distortion due to both random laser PN and the effect of the residual pump-phase modulation is partly removed from the input signal. From the spectrum of the estimated PN after the first stage (Fig. 2(b)), we can see that the traditional BPS method allows us to estimate the frequencies f_1 and f_2 of the two RF tones modulating the pumps and also their mixing products. However, due to its decision-directed architecture, the accuracy of this BPS estimation in the presence of large pump-phase mismatches may significantly degrade, especially for the higher-order QAM signals which have smaller PN tolerance. The red signal points in the constellation diagram after the first PN compensation block in Fig. 2(a) represent the 16-QAM symbols that are in error as a result of direct decision. We can see that the majority of these wrong symbols belong to the outer rings of the signal constellation, reflecting the fact that the outer constellation symbols are more susceptible to PN than the inner ones. This reduced PN tolerance becomes more prevalent with increasing signal modulation order.

Optics EXPRESS

Therefore, in order to track and compensate the remaining phase distortion after the first stage of PN compensation, we propose here to use a second PN compensation stage. Taking advantage of the partial suppression of the phase distortion induced by imperfect pump counter-phasing which is accomplished by the first stage, we can approximate the general pump phase contribution to the idler phase in Eq. (2) by the sum of the two RF modulating signals: $\phi_m \sim a_1 \cos(2\pi f_1 t + \theta_1) + a_2 \cos(2\pi f_2 t + \theta_2)$. Indeed, the frequency components contributed by the nonlinear terms in Eq. (2) are numerous and appear as additional white noise, and so we assume that the first stage can compensate for these. We can therefore focus the second PN compensation block on the dominant residual pump-phase modulation components, which occur at the original phase-modulation drive frequencies. Hence in this block, Algorithm 1 is executed to find the optimum amplitudes a_i and angles θ_i of the tone signals. For each tone, a blind grid search (10×10) is performed with a step size of 0.02 rad and 0.63 rad for the amplitude and angle, respectively. The number of preset values and the step sizes are chosen to balance the algorithm's performance with its complexity. The latter is discussed below. Inside each iteration, a test cosine wave c is constructed (line 6 in Algorithm 1), which is then used to phase-rotate the extracted QAM symbols. Then all rotated symbols are fed into a decision circuit and the square distances e to the closest constellation points are calculated in the complex plane (line 9). After the two-dimensional sweeping, the optimum amplitudes and angles of the cosine waves are determined by searching the minimum sum of distance values (line 17). Finally, the optimum phase modulation is used to rotate the signal after the first stage of PN compensation.

We can easily see that the computational complexity of Algorithm 1 scales as the number of preset values of the amplitude and angle of the tones that are evaluated in the *for* loops (lines 4 and 5). For simplicity, we can use here the number of real-valued multiplications as a figure of merit considering that the complexity of other operations such as additions and direct decisions take a small proportion of the total complexity. For each *for* run, the construction of the test symbols (line 7) and the error calculation require 1024 and 512 real-valued multipliers, respectively. Note that the the test cosine wave (line 6) can be implemented efficiently by using a look-up table. Therefore, the overall computational complexity of Algorithm 1 can be estimated as $2N_aN_\theta(1024 + 512)$, where factor 2, N_a and N_θ represent the number of frequencies, amplitudes and angles considered in the three *for* loops, respectively.

Algorithm 1 Pump counter-phasing induced PN extraction

1: *Input*:
2: $\boldsymbol{x}, \boldsymbol{d}_{\text{pilot}}, \boldsymbol{t}, \boldsymbol{f}$ ▷ QAM data after first stage PN compensation, pilot vector, time vector and modulation frequency vector.
3: **for** $f_i = 1 : \text{length}(\boldsymbol{f})$ **do**
4: **for** $a = 0 : 0.02 : 0.2$ **do**
5: **for** $\theta = -\pi : (2\pi/10) : \pi$ **do**
6: $\boldsymbol{c} = a\cos(2\pi \boldsymbol{f}(i)\boldsymbol{t} + \theta)$
7: $\boldsymbol{x}_{\text{test}} \leftarrow \boldsymbol{x}e^{-j\boldsymbol{c}}$
8: **if** pilot-free **then**
9: $\sum \boldsymbol{e} \leftarrow \sum |\boldsymbol{x}_{\text{test}} - \lfloor \boldsymbol{x}_{\text{test}} \rfloor_{\text{D}}|^2$
10: ▷ $\lfloor\rfloor_{\text{D}}$: direct-decision
11: **end if**
12: **if** pilot-aided **then**
13: $\sum \boldsymbol{e} \leftarrow |\boldsymbol{x}_{\text{test}} - \boldsymbol{d}_{\text{pilot}}|^2$
14: **end if**
15: **end for**
16: **end for**
17: $(a_i, \theta_i) \leftarrow \underset{(a,\theta)}{\text{argmin}}(\boldsymbol{e})$
18: **end for**
19: **return** $\sum a_i \cos(2\pi f_i \boldsymbol{t} + \theta_i)$

Optics EXPRESS

Because of the BPS in the first stage, the performance of the two-stage scheme relies on direct-decision operators. As such, the stronger the modulation index and/or pump-phase mismatch in the pump phase contribution to the signal phase, the more likely the wrong decision is made by the algorithm, especially with high-order (64- and beyond) QAM where the Euclidean distances between constellation points are small. To make the scheme applicable to high-order QAM, we also deploy pilot-aided PN estimation. In this case, the first stage of PN compensation is a conventional pilot-aided algorithm [12,13], and the QAM extraction module in the second stage is replaced by a pilot extraction module. Therefore, the PN in the first stage is now estimated from a window of 8 pilot symbols as $\delta\hat{\phi} = \frac{1}{8}\arg(\sum_{k=1}^{8} \frac{y[k]d[k]^*_{\text{pilot}}}{|y[k]||d[k]_{\text{pilot}}|})$, and the error calculation in Algorithm 1 is no longer based on direct symbol decision but on the extracted pilots (line 13).

3. Experimental setup

The schematic representation of the dual-polarisation 28-Gbaud 16/64/256-QAM system that is used to validate the proposed PN compensation method is shown in Fig. 3. At the transmitter, ~ 60000 random QAM symbols are generated for each polarisation. To test the two-stage pilot-aided scheme with 64- and 256-QAM, the complex QAM payload is time-multiplexed with 4-QAM pilots regularly. We deploy 5% pilot overhead, i.e., 1 pilot in every 19 QAM data. The data is then up-sampled at a rate of 2 samples per symbol and pulse-shaped using a root-raised-cosine filter with a 0.1 roll-off factor. A special preamble of length 9 ns (equivalent to 256-symbol duration) and consisting of two repeated parts [22] is inserted at the beginning of each ~ 2.25 μs-long frame to aid the frame synchronisation at the receiver. The signal is loaded into an arbitrary waveform generator (AWG; 4-channel, 8-bit digital-to-analogue converter with 56-GSa/s sample rate from Keysight) and subsequently converted into the optical domain by a commercial multi-format optical transmitter (~ 100-kHz laser linewidth on 192.4 THz). An erbium-doped fibre amplifier (EDFA) is used to control the launch signal power.

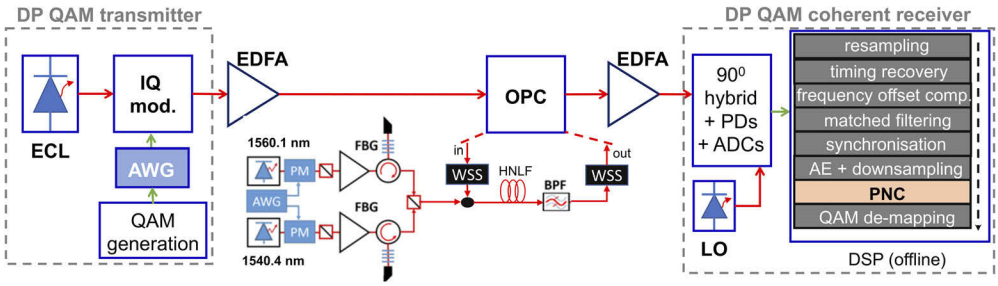

Fig. 3. Experimental setup showing the dual-polarisation 28-Gbaud 16/64/256-QAM transmitter, the dual-pump polarisation-insensitive OPC device, the coherent receiver, and the offline DSP equipped with the proposed dual-stage PN compensation scheme. ECL: external cavity laser, mod.: modulator, AWG: arbitrary waveform generator, EDFA: erbium-doped fibre amplifier, OPC: optical phase conjugation, PM: phase modulator, PC: polarisation controller, FBG: fibre Bragg grating, PBC: polarisation beam combiner, BPF: optical band-pass filter, WSS: wave selective switch, LO: local oscillator, PDs: photodetectors, ADCs: analogue-to-digital converters, DSP: digital signal processing, AE: adaptive equaliser, PNC: phase-noise compensation.

The signal is conjugated through a polarisation-insensitive dual-band OPC with orthogonally polarised pumps spectrally located at 1540.4 nm and 1560.1 nm, and with laser linewidth ~ 30 kHz. The details of the OPC setup can be found in [18,23]. One signal band only is used in this experiment. Two RF tones at frequencies f_1 and f_2 are generated by an AWG and used to independently phase-modulate the pump lasers via optical phase modulators. First, we adjust

Optics EXPRESS

the amplitudes and phases of the RF tones to minimise the transfer of phase modulation from the pumps to the generated idler, that is, to equalise the amplitudes of the pump phases and adjust the counter-dithering phase offset $\delta\theta = \theta_2 - (\theta_1 + 180^\circ)$ to zero so that a counter-dithering condition for the pumps is satisfied. Here, θ_i denotes the phase of the RF tones driving each phase modulator $i = 1, 2$. The transceiver's performance in this operational condition is recorded for reference. Then, we intentionally increase the phase mismatch $\delta\theta$ up to 10° by tuning the phase offset of the RF tones. The HNLF is 100 m long, and the nominal values of the fibre attenuation coefficient, Kerr nonlinearity coefficient, zero-dispersion wavelength, and dispersion slope are $\alpha = 1.2$ dB/km, $\gamma = 21.4\,(\mathrm{W}\cdot\mathrm{km})^{-1}$, 1550 nm, and $0.041\,\mathrm{ps}/(\mathrm{nm}^2\cdot\mathrm{km})$, respectively.

Detection of the conjugated copy of the signal is performed with a typical intra-dyne coherent receiver using a local oscillator with ~ 100-kHz linewidth on 193.1 THz. The local oscillator is combined with the data in a 90° optical hybrid. Four balanced photodetectors are connected to the hybrid outputs, and a real-time sampling scope (100-GS/s sample rate, 33-GHz analogue bandwidth) is used as analogue-to-digital converter. A standard DSP procedure for data recovery [24] is implemented offline on a desktop computer. The DSP starts with re-sampling the digital signal at 2 samples per symbol. Timing recovery and frequency-offset error correction are performed using a Gardner phase detector (window size of 1024) and a conventional Fourier-transform-based method (window size of 4096) [25,26], respectively. After matched filtering, frame synchronisation is achieved by use of the Schmidl-Cox algorithm [22]. An adaptive butterfly-structure equaliser (15 taps) demultiplexes the dual-polarisation fields and compensates linear effects. The signal is then down-sampled to 1 sample per symbol before being fed into the proposed two-stage PN compensation module to remove laser and imperfect pump counter-phasing induced phase distortions from it. At the output of the PN compensation module, the pilot symbols are removed before QAM de-mapping. The recovered QAM symbols together with the transmitted symbols are used to measure an effective SNR defined as $\mathrm{SNR} = \mathbb{E}_k[|x[k]|^2]/\mathbb{E}_k[|\hat{y}[k] - x[k]|^2]$, where $x[k]$ and $\hat{y}[k]$ are the respective transmitted and received QAM symbols at the time instance k and $\mathbb{E}$ is the expectation operator [27].

4. Results and discussion

To evaluate the effectiveness of the proposed two-stage PN compensation scheme, we set the OPC transceiver to operate at an optical SNR of ~ 36 dB under optimum pump counter-phasing ($\delta\theta = 0^\circ$), thus achieving an optimum effective SNR after DSP of ~ 20-21 dB. Then we assess the performance of PN compensation in terms of effective SNR for varying pump-phase mismatch $\delta\theta$. The results obtained from the experiment and numerical simulation of the model system shown in Fig. 3 are summarised in Fig. 4. We observe that the performance of the conventional PN compensation stage degrades significantly under the impact of imperfect pump counter-phasing for all QAM modulation orders: more than 1-dB SNR penalty is observed at a pump-phase mismatch of only 3°. In contrast, the proposed two-stage scheme can tolerate pump-phase mismatches of up to 8° under the operating condition of less than 1-dB SNR penalty. At $\delta\theta = 8^\circ$, the two-stage scheme achieves a SNR improvement of at least 4 dB over conventional PN compensation for all QAM modulation orders.

Comparing the results for 16- and 64-QAM (panels (a) and (b) of Fig. 4, respectively), we can see that the improvement in performance of the pilot-free two-stage PN compensation scheme relative to its one-stage counterpart is significantly reduced for high-order QAM, as expected. We also note that the one-stage pilot-aided method is not capable to cope with the PN generated by imperfect pump counter-phasing for 64-QAM, thereby impelling us to deploy two-stage pilot-aided PN compensation in this QAM system. This is confirmed by the 64-QAM constellation diagrams recorded at $\delta\theta = 8^\circ$, which are shown in Figure 4(d): the number of symbol changes in constellation aggregation (red marks) is only slightly decreased by the application of pilot-aided one-stage PN compensation (constellation marked as *) as compared

Optics EXPRESS

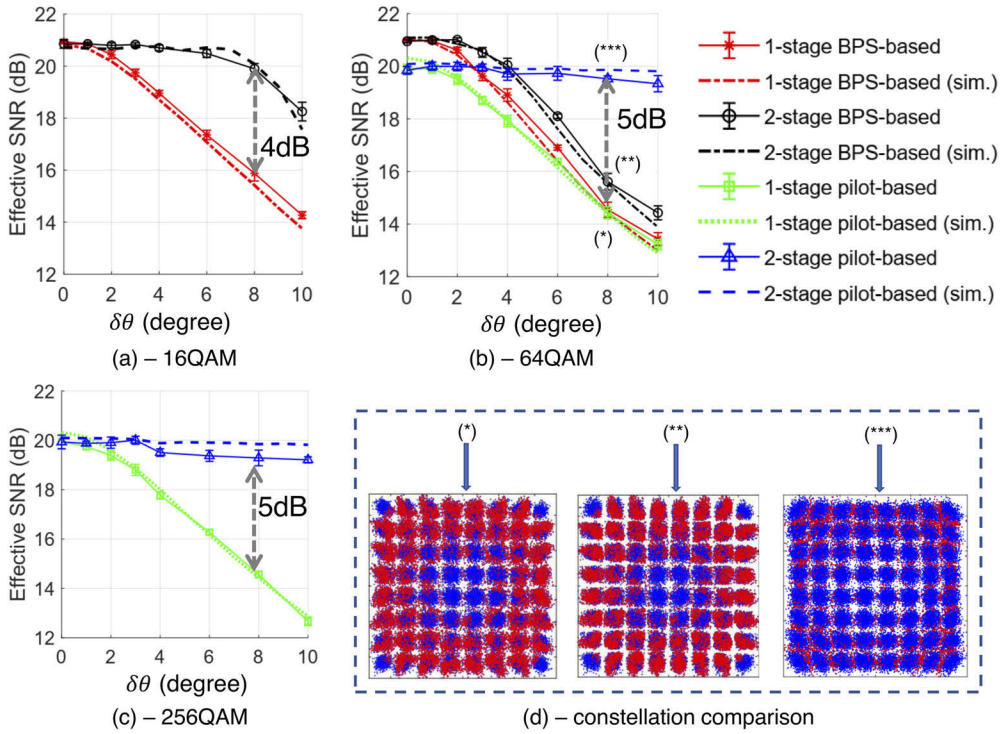

Fig. 4. Performance of the proposed PN compensation approach. (a)–(c): Effective SNR (dB) versus pump-phase mismatch, $\delta\theta$ (degree), for 16-, 64- and 256-QAM systems after one- and two-stage pilot-free PN compensation (red and black curves, respectively) and one-and two-stage pilot-aided PN compensation (green and blue curves, respectively). The experimental and numerical results are represented by solid and dashed curves, respectively. (d): 64-QAM constellation diagrams at $\delta\theta = 8°$ for one-stage pilot-free ((*)), two-stage pilot-free ((**)), and two-stage pilot-aided ((***)) PN compensation.

to the pilot-free one-stage scheme (constellation **). In contrast, almost all phase errors vanish after using the two-stage pilot-aided scheme (constellation ***), leading to a SNR enhancement of ~ 5 dB (Fig. 4(b)). Further, it is worth noting that for pump-phase mismatches $\delta\theta$<2° the pilot-aided PN compensation method, either one- or two-stage, features a SNR degradation of ~ 1 dB relative to the blind approach. This is explained by the fact that in the region of small $\delta\theta$ the system's performance is dominated by laser PN, and the achievable SNR by conventional PN compensation scales as the inverse product of the symbol duration and laser linewidth [11,12]. This product is much larger for the pilot-aided schemes, thus resulting in increased SNR penalty.

For the 256-QAM system, only the performances of the pilot-aided methods are compared in Fig. 4(c). We observe that in a similar manner to the 64-QAM case, at $\delta\theta = 8°$ the two-stage scheme has a SNR improvement of ~ 5 dB relative to the one-stage scheme. These results confirm that the proposed two-stage PN compensation approach maintains its advantages with increasing modulation order. Further, we observe in Fig. 4 that the performance of the PN compensation schemes evaluated by numerical simulation of the model system generally matches very well the performance calculated from experimental data for all QAM modulation orders, although this agreement is slightly worse in the 256-QAM case due to the more severe impact of the transceiver's implementation [28]. The good agreement between the numerical simulation and experimental results corroborates the soundness of our findings and allows us to use numerical

Optics EXPRESS

simulations to study the behaviour of the proposed two-stage PN compensation scheme under different pump settings in the OPC device.

Figure 5 illustrates the impact of the number of preset values of the tone's amplitude and angle evaluated in Algorithm 1 on the performance of the proposed PN compensation scheme when the method is applied to all the QAM formats being studied under the same pump-phase mismatch of 4°. For simplicity, we use the same number of preset values for the tone's amplitude and angle. We can see that the system's performance improves with increasing number of tested parameter values (i.e., with higher resolution) up to $N_a = N_\theta = 10$. Nevertheless, there is almost no additional benefit from increasing N_a and N_θ further. Thus, we can conclude that Algorithm 1 costs 307200 multipliers for its implementation.

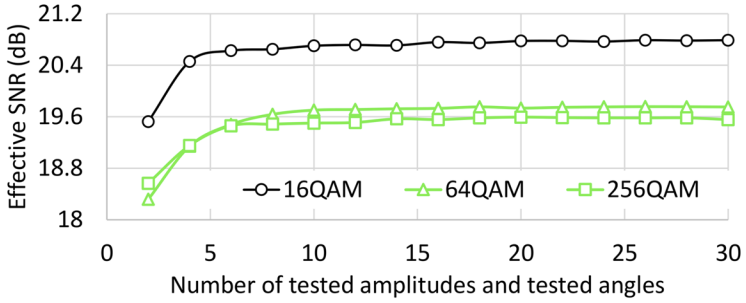

Fig. 5. Performance of the two-stage PN compensation scheme versus number of amplitude and angle steps in Algorithm 1 for for 16-, 64- and 256-QAM at 4° pump-phase mismatch. The black and green curves represent the performances of BPS- and pilot-based PN compensation, respectively.

The transfer of laser PN from the pumps to the conjugated signal is also an important limitation to the realisation of practical OPC systems. To study the impact of both pump laser PN and imperfections in the pump-phase modulation scheme on the performance of the proposed PN compensation scheme, we simulate numerically an OPC system with artificially varying laser linewidth and pump-phase mismatch. Figure 6 shows the tolerance of the scheme to the joint effects of pump laser linewidth and pump-phase mismatch when the SNR penalty is constrained to less than 1 dB. Here the SNR penalty represents the additional SNR that is required to reach the tested bit-error rate (BER) thresholds of $\sim 3.8 \times 10^{-3}$, $\sim 2 \times 10^{-2}$ and $\sim 4.5 \times 10^{-2}$ for 28 Gbaud 16-, 64- and 256-QAM, respectively. The simulated SNR values recorded at these BER thresholds with an ideal OPC device ($\delta\nu = 0$ Hz and $\delta\theta = 0°$) are 16 dB, 19.5 dB and 23 dB for the 16-, 64- and 256-QAM systems, respectively. The results shown in Fig. 6 indicate that the proposed two-stage approach, either pilot-free (16- and 64-QAM) or pilot-aided (64- and 256-QAM) is capable to compensate the phase distortion arising from imperfect pump phase modulation for pump phase-mismatch values of up to 3° for all QAM systems being studied. At pump-phase mismatches $\delta\theta \leq 3°$, the tolerable limits of pump laser linewidth are $\sim$ 1 MHz, 400 kHz and 200 kHz for the 16-, 64- (with pilot-aided PN compensation) and 256-QAM systems. In general, the higher the modulation order and/or the larger the pump-phase mismatch, the lower the tolerance to pump laser linewidth. It is worth to note that the tolerance of the pilot-free PN compensated 16-QAM system to laser linewidth decreases quickly for pump-phase mismatches beyond 7° as a result of the decision-directed architecture of BPS. Direct decision has a stronger impact on the PN compensated 64-QAM system for which the tolerance to pump laser linewidth starts to fall when $\delta\theta$ is just above 2°.

We have also verified experimentally that the proposed PN compensation method works well when the OPC transceiver is operated at different optical SNR levels, with the results confirming that the performance of the second stage is relatively insensitive to the pump-phase mismatch

Optics EXPRESS

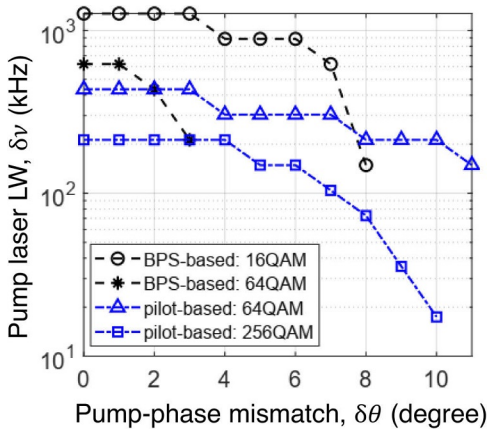

Fig. 6. Tolerance of the two-stage PN compensation scheme to pump-phase mismatch and pump laser linewidth for 16-, 64- and 256-QAM with the constraint of <1 -dB SNR penalty at the BER thresholds of $\sim 3.8 \times 10^{-3}$, $\sim 2 \times 10^{-2}$ and $\sim 4.5 \times 10^{-2}$, respectively.

level (as seen in Fig. 4), thereby leading to an effective SNR gain over the first stage which increases with higher optical SNR and stronger residual pump dithering [29]. Nevertheless, we should note that some complicating effects may arise when applying the compensation scheme in a transmission setup with mid-link spectral inversion by OPC. Specifically, the residual pump dithering will make the fibre chromatic dispersion subtly different in the two halves of the link, which, in turn, will impair the dispersion compensation by the OPC, and so the nonlinearity compensation will be degraded too. These effects are similar to equalisation-enhanced PN [30]. We have used numerical simulations to study the behaviour of the PN compensation scheme under an inline EDFA transmission configuration with mid-link OPC. The fibre channel includes 4 or 8 identical spans, each of 100-km standard single-mode fibre (α = 0.2 dB/km, group-velocity dispersion = $-21.7\,\mathrm{ps}^2/\mathrm{km}$, $\gamma = 1.3\,(\mathrm{W}\cdot\mathrm{km})^{-1}$) followed by an EDFA (noise figure = 6 dB) to compensate for the fibre loss. The results shown in Fig. 7 for the 256-QAM signal highlight that

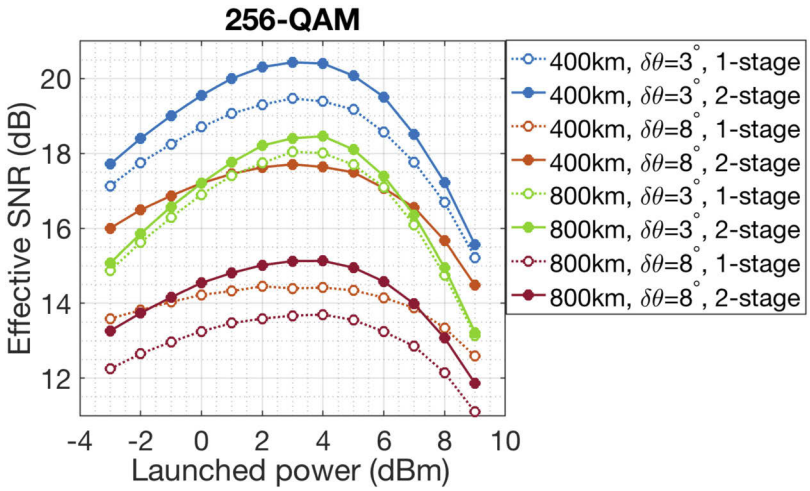

Fig. 7. Effective SNR versus launched power after one- and two-stage PN compensation at $\delta\theta = 3°$ and 8° for 256-QAM transmission over 400-km and 800-km of fibre link.

Optics EXPRESS

the second stage of PN compensation always outperforms the first stage and brings about a SNR advantage at the optimum launched power of ~ 1 dB and ~ 0.5 dB after 400-km and 800-km of fibre link, respectively, in the presence of low residual pump dithering. This advantage increases to ~ 3 dB (after 400 km) and ~ 1.5 dB (after 800 km) under severe residual dithering. However, as expected, the benefit of the method is degraded with respect to the back-to-back configuration and diminishes with longer transmission. This is ascribed to the impact of fibre dispersion in the second half of the link. Optimisation of the PN compensation scheme within the transmission scenario will be investigated in a future work.

5. Conclusion

We have developed a new two-stage DSP scheme to compensate the phase distortion induced by deviations from ideal pump counter-phasing for dual-pump OPC of high-order QAM signals. We have demonstrated numerically and experimentally that the proposed approach achieves large SNR improvement relative to conventional PN compensation when it is used with 16/64/256-QAM signals in the presence of severe imperfections in the pump-modulation scheme. Therefore, our results indicate that a slightly increased complexity of the offline DSP in coherent optical systems deploying OPC may be a worthy price to pay to avoid precise calibration of the pump-phase modulation scheme. We should note that in our experiment, the SNR is such that there is little penalty from the residual pump-phase modulation when the system is fully optimised, due to the OPC conversion efficiency/insertion loss. However, we believe that the technique presented in this paper may firstly allow the applied pump phase modulation to be increased, improving the conversion efficiency and secondly, reduce residual phase modulation penalties for OPC systems with lower optical SNR penalties. It should also apply to the single pump OPC, greatly relaxing the constraint on the phase modulation index. Investigating these issues will be the subject of future work. Future research will also include the optimisation of the PN compensation in OPC-assisted transmission setups. Furthermore, a closely related line of work will be the investigation and optimisation of a compensation scheme in which part of the degradation in the nonlinearity compensation by the OPC that results from the symmetry breakage in the transmission link caused by the residual pump dithering is offset at the transmitter.

Funding. This work was supported by the UK EPSRC (Engineering and Physical Sciences Research Council) (EP/R035342/1 - TRANSNET, EP/S003436/1 - PHOS, EP/S016171/1 - EEMC).

Disclosures. The authors declare no conflicts of interest.

Data availability. Data underlying the results presented in this paper may be obtained from the authors upon reasonable request.

References

1. A. D. Ellis, M. E. McCarthy, M. A. Z. Al-Khateeb, M. Sorokina, and N. J. Doran, "Performance limits in optical communications due to fiber nonlinearity," Adv. Opt. Photonics **9**(3), 429–503 (2017).
2. M. A. Z. Al-Khateeb, M. E. McCarthy, C. Sánchez, and A. D. Ellis, "Nonlinearity compensation using optical phase conjugation deployed in discretely amplified transmission systems," Opt. Express **26**(18), 23945–23959 (2018).
3. J. B. Coles, B. P.-P. Kuo, N. Alic, S. Moro, C.-S. Bres, J. M. Chavez Boggio, P. A. Andrekson, M. Karlsson, and S. Radic, "Bandwidth-efficient phase modulation techniques for stimulated Brillouin scattering suppression in fiber optic parametric amplifiers," Opt. Express **18**(17), 18138–18150 (2010).
4. M. E. McCarthy, S. Sygletos, N. Mac Suibhne, M. Tan, M. Stephens, I. D. Phillips, P. Harper, N. J. Doran, and A. D. Ellis, "Challenges of developing non-linear devices to achieve the linear Shannon limit," In: *16th International Conference on Transparent Optical Networks (ICTON)* (Graz, Austria, 2014), 1–6.
5. Y. Liu, Z. Lv, Y. Dong, and Q. Li, "Research on stimulated Brillouin scattering suppression based on multi-frequency phase modulation," Chin. Opt. Lett. **7**(1), 29–31 (2009).
6. A. Flores, C. Robin, A. Lanari, and I. Dajani, "Pseudo-random binary sequence phase modulation for narrow linewidth, kilowatt, monolithic fiber amplifiers," Opt. Express **22**(15), 17735–17744 (2014).
7. R. Elschner, C.-A. Bunge, B. Hüttl, A. Gual i Coca, C. Schmidt-Langhorst, R. Ludwig, C. Schubert, and K. Petermann, "Impact of pump-phase modulation on FWM-based wavelength conversion of D(Q)PSK signals," IEEE J. Sel. Top. Quantum Electron. **14**(3), 666–673 (2008).

Optics EXPRESS

8. M.-C. Ho, M. E. Marhic, K. K. Y. Wong, and L. G. Kazovsky, "Narrow-linewidth idler generation in fiber four-wave-mixing and parametric amplification by dithering two pumps in opposition of phase," J. Lightwave Technol. **20**(3), 469–476 (2002).
9. R. Elschner, C.-A. Bunge, and K. Petermann, "Co- and counterphasing tolerances for dual-pump parametric λ-conversion of D(Q)PSK signals," IEEE Photonics Technol. Lett. **21**(11), 706–708 (2009).
10. E. Ip and J. M. Kahn, "Feedforward carrier recovery for coherent optical communications," J. Lightwave Technol. **25**(9), 2675–2692 (2007).
11. T. Pfau, S. Hoffmann, and R. Noe, "Hardware-efficient coherent digital receiver concept with feedforward carrier recovery for *M*-QAM constellations," J. Lightwave Technol. **27**(8), 989–999 (2009).
12. G. Colavolpe, T. Foggi, E. Forestieri, and M. Scondini, "Impact of phase noise and compensation techniques in coherent optical systems," J. Lightwave Technol. **29**(18), 2790–2800 (2011).
13. S. Randel, S. Adhikari, and S. L. Jansen, "Analysis of RF-Pilot-Based Phase Noise Compensation for Coherent Optical OFDM Systems," IEEE Photonics Technol. Lett. **22**(17), 1288–1290 (2010).
14. R. Elschner, T. Richter, L. Molle, C. Schubert, and K. Petermann, "Single-pump FWM-wavelength conversion in HNLF using coherent receiver-based electronic compensation," In: *36th European Conference and Exhibition on Optical Communication (ECOC)*, Torino, Italy (2010), paper number P3.17.
15. S. Ortega Zafra, X. Pang, G. Jacobsen, S. Popov, and S. Sergeyev, "Phase noise tolerance study in coherent optical circular QAM transmissions with Viterbi-Viterbi carrier phase estimation," Opt. Express **22**(25), 30579–30585 (2014).
16. M. Lax, "Classical noise. V. Noise in self-substained oscillators," Phys. Rev. **160**(2), 290–307 (1967).
17. C. H. Henry, "Theory of the linewidth of SC Lasers," IEEE J. Quantum Electron. **18**(2), 259–264 (1982).
18. M. A. Z. Al-Khateeb, M. Tan, Md. A. Iqbal, A. Ali, M. E. McCarthy, P. Harper, and A. D. Ellis, "Experimental demonstration of 72% reach enhancement of 3.6 Tbps optical transmission system using mid-link optical phase conjugation," Opt. Express **26**(18), 23960–23969 (2018).
19. J. C. Pedro and S. A. Maas, "A Comparative overview of microwave and wireless power amplifier behavioral modeling approaches," IEEE Trans. Microwave Theory Tech. **53**(4), 1150–1163 (2005).
20. C. J. McKinstrie, S. Radic, and A. R. Chraplyvy, "Parametric amplifiers driven by two pump waves," IEEE J. Sel. Top. Quantum Electron. **8**(3), 538–547 (2002).
21. G. P. Agrawal, *Nonlinear Fiber Optics*, 3th ed. (Academic Press, San Diego, CA, 2001).
22. T. M. Schmidl and D. C. Cox, "Robust frequency and timing synchronization for OFDM," IEEE Trans. Commun. **45**(12), 1613–1621 (1997).
23. A. A. I. Ali, M. Al-Khateeb, T. Zhang, F. Ferreira, and A. Ellis, "Enhanced nonlinearity compensation efficiency of optical phase conjugation system," In: *Optical Fiber Communications Conference and Exhibition (OFC)*, San Diego, CA, USA (2019), pp. 1–3.
24. J. Savory Seb, "Digital filters for coherent optical receivers," Opt. Express **16**(2), 804–817 (2008).
25. X. Zhou, "Efficient clock and carrier recovery algorithms for single-carrier coherent optical systems: A systematic review on challenges and recent progress," IEEE Signal Process. Mag. **31**(2), 35–45 (2014).
26. M. Selmi, Y. Jaouen, and P. Ciblat, "Accurate digital frequency offset estimator for coherent polmux qam transmission systems," In: *35th European Conference and Exhibition on Optical Communication (ECOC)*, Vienna, Austria (2009), pp. 1–2.
27. R. Maher, A. Alvarado, D. Lavery, and P. Bayvel, "Increasing the information rates of optical communications via coded modulation: A study of transceiver performance," Sci. Rep. **6**(1), 21278 (2016).
28. T. T. Nguyen, T. Zhang, E. Giacoumidis, A. A. I. Ali, M. Tan, P. Harper, L. P. Barry, and A. D. Ellis, "Coupled transceiver-fiber nonlinearity compensation based on machine learning for probabilistic shaping system," J. Lightwave Technol. **39**(2), 388–399 (2021).
29. T. T. Nguyen, S. Boscolo, A. A. I. Ali, M. Tan, S. Sygletos, S. Takasaka, R. Sugizaki, and A. D. Ellis, "Digital compensation of residual pump dithering in optical phase conjugation of high-order QAM," *Optical Networking and Communication Conference & Exhibition (OFC)*, San Francisco, California, USA (2021), Accepted.
30. W. Shieh and K.-P. Ho, "Equalization-enhanced phase noise for coherent-detection systems using electronic digital signal processing," Opt. Express **16**(20), 15718–15727 (2008).